Organic Functionalization and Morphology Control of Mesoporous Silicas via a Co-Condensation Synthesis Method

Seong Huh, Jerzy W. Wiench, Ji-Chul Yoo,† Marek Pruski, and Victor S.-Y. Lin*

Department of Chemistry, and Ames Laboratory-U.S. Department of Energy, Iowa State University, Ames, Iowa 50011-3111

Received October 10, 2002. Revised Manuscript Received July 8, 2003

A series of new mesoporous silica materials with MCM-41 type of structure containing a homogeneous layer of organic functional groups inside the pores was prepared using a co-condensation method under low surfactant concentration condition. This reproducible synthetic approach resulted in high surface coverage with several functional groups such as a primary amine, secondary amine, urea, isocyanate, vinyl, and nitrile. In addition, the presence of organoalkoxysilane precursors during the base catalyzed condensation greatly influenced the final particle shape. By changing the precursor or its concentration, the particle morphology was tuned to various shapes, including spheres, tubes, and rods of various dimensions. The synthetic procedures that gave rise to the specific particle morphologies were investigated and the mechanism responsible for shape control was postulated. The structure and functionality of these materials were characterized by field-emission scanning electron microscopy, transmission electron microscopy, solid-state NMR spectroscopy, thermogravimetric analysis, and nitrogen adsorption and desorption studies (BET isotherms and BJH pore size distribution measurements).

Introduction

Since the discovery of surfactant micelle-templated synthesis of mesoporous silica materials, such as MCM-41/48,[1,2] SBA-15,[3] MSU-n,[4] KIT-1,[5] and FSM-16,[6] many research efforts have focused on (i) preparing the organic/inorganic hybrids through *functionalization* of the exterior and/or interior surfaces, and (ii) controlling the *particle morphology*. The success of such investigations will prompt the utilization of these materials in separation,[7] sensor design,[8] catalysis,[9] and drug delivery.[10]

Scheme 1

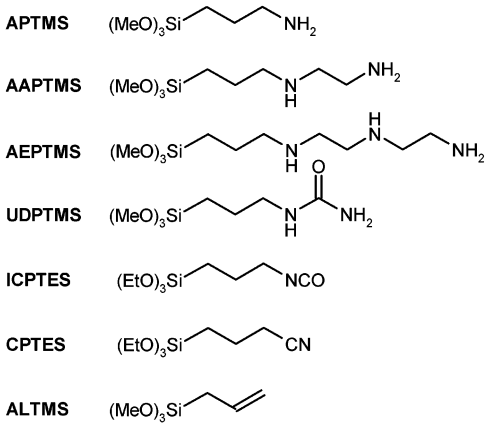

Although numerous synthetic approaches have been pursued and significant progress has been made in *functionalization* of the MCM silicas with various organic groups, the current state-of-the-art methods,

* To whom correspondence should be addressed. Phone: (515) 294-3135. E-mail: vsylin@iastate.edu.

† Current address: A. E. Team, R&D Center, Samsung Electro-Mechanics Co., Ltd. Suwon, Kyunggi-Do, 442-743 Korea.

(1) Beck, J. S.; Vartuli, J. C.; Roth, W. J.; Leonowicz, M. E.; Kresge, C. T.; Schmitt, K. D.; Chu, C. T. W.; Olson, D. H.; Sheppard, E. W.; McCullen, S. S. B.; Higgins, J. B.; Schlenker, J. L. *J. Am. Chem. Soc.* **1992**, *114*, 10834−10843.

(2) Kresge, C. T.; Leonowicz, M. E.; Roth, W. J.; Vartuli, J. C.; Beck, J. S. *Nature (London)* **1992**, *359*, 710−712.

(3) Zhao, D.; Feng, J.; Huo, Q.; Melosh, N.; Frederickson, G. H.; Chmelka, B. F.; Stucky, G. D. *Science (Washington, D. C.)* **1998**, *279*, 548−552.

(4) Bagshaw, S. A.; Prouzet, E.; Pinnavaia, T. J. *Science (Washington, D. C.)* **1995**, *269*, 1242−1244.

(5) Ryoo, R.; Kim, J. M.; Ko, C. H.; Shin, C. H. *J. Phys. Chem.* **1996**, *100*, 17718−17721.

(6) Inagaki, S.; Koiwai, A.; Suzuki, N.; Fukushima, Y.; Kuroda, K. *Bull. Chem. Soc. Jpn.* **1996**, *69*, 1449−1457.

(7) (a) Dai, S.; Burleigh, M. C.; Shin, Y.; Morrow, C. C.; Barnes, C. E.; Xue, Z. *Angew. Chem., Int. Ed.* **1999**, *38*, 1235−1239. (b) Lin, Y.; Fryxell, G. E.; Wu, H.; Engelhard, M. *Environ. Sci. Technol.* **2001**, *35*, 3962−3966. (c) Yoshitake, H.; Yokoi, T.; Tatsumi, T. *Chem. Mater.* **2003**, *15*, 1713−1721. (d) Yoshitake, H.; Yokoi, T.; Tatsumi, T. *Bull. Chem. Soc. Jpn.* **2003**, *76*, 847−852. (e) Hossain, K. Z.; Mercier, L. *Adv. Mater. (Weinheim, Ger.)* **2002**, *14*, 1053−1056.

(8) (a) Lin, V. S. Y.; Lai, C.-Y.; Huang, J.; Song, S.-A.; Xu, S. *J. Am. Chem. Soc.* **2001**, *123*, 11510−11511. (b) Burleigh, M. C.; Dai, S.; Hagaman, E. W.; Lin, J. S. *Chem. Mater.* **2001**, *13*, 2537−2546.

(9) (a) Soler-Illia Galo, J. d. A. A.; Sanchez, C.; Lebeau, B.; Patarin, J. *Chem. Rev.* **2002**, *102*, 4093−4138. (b) Stein, A. *Adv. Mater. (Weinheim, Ger.)* **2003**, *15*, 763−775. (c) Davis, M. E. *Nature (London)* **2002**, *417*, 813−821. (d) Corma, A. *Chem. Rev.* **1997**, *97*, 2373−2419. (e) Price, P. M.; Clark, J. H.; Macquarrie, D. J. *Dalton* **2000**, 101−110. (f) Ying, J. Y.; Mehnert, C. P.; Wong, M. S. *Angew. Chem., Int. Ed.* **1999**, *38*, 56−77. (g) Sayari, A. *Chem. Mater.* **1996**, *8*, 1840−1852. (h) Moller, K.; Bein, T. *Chem. Mater.* **1998**, *10*, 2950−2963.

(10) Lai, C.-Y.; Trewyn, B. G.; Jeftinija, D. M.; Jeftinija, K.; Xu, S.; Jeftinija, S.; Lin, V. S. Y. *J. Am. Chem. Soc.* **2003**, *125*, 4451−4459.

10.1021/cm0210041 CCC: $25.00
Published on Web 10/03/2003

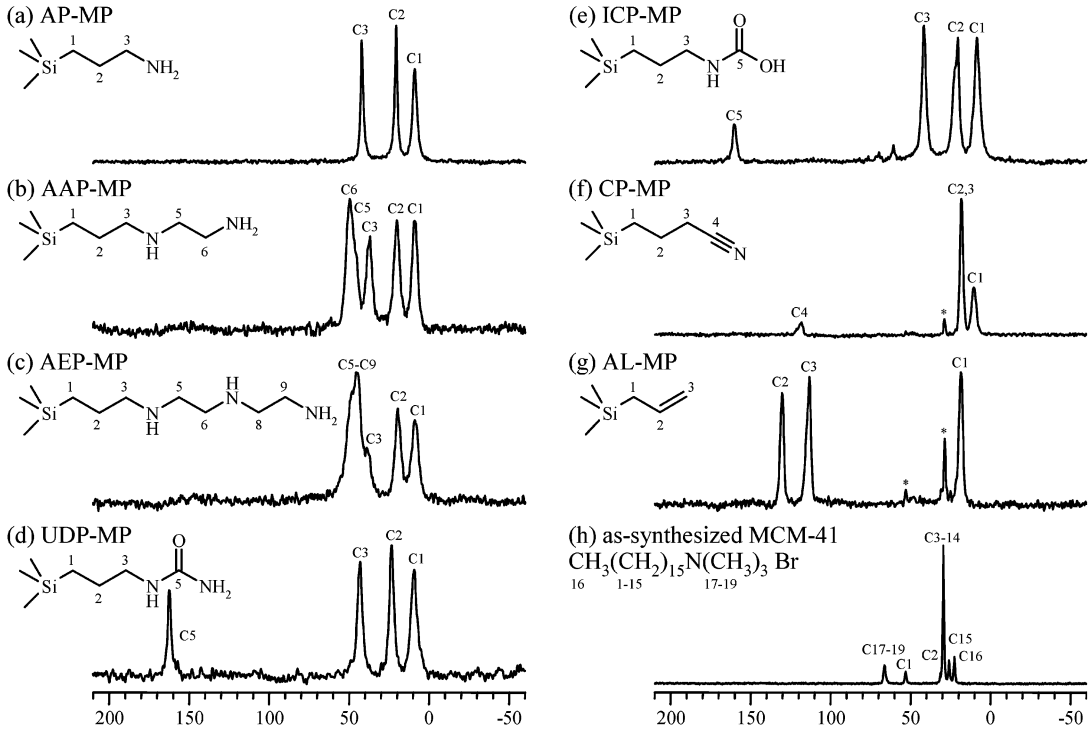

Figure 1. $^{1}H \rightarrow {}^{13}C$ CPMAS spectra of AP-MP (a), AAP-MP (b), AEP-MP (c), UDP-MP (d), ICP-MP (e), CP-MP (f), AL-MP (g), and s-MCM-41 (h) using CP contact time of 0.4 (spectra a−c and h) or 1.5 ms (spectra d−g). Asterisks mark positions of residual surfactant carbons present in spectra f and g. Note that spectrum (e) represents the propyl-carbamic acid group formed during the synthesis of ICP-MP by base-catalyzed hydrolysis of isocyanopropyl group.

Table 1. ^{13}C Chemical Shifts (δ_C, in ppm from TMS) of Organic Groups Obtained from $^{1}H \rightarrow {}^{13}C$ CPMAS Spectra

AP-MP		AAP-MP		AEP-MP		UDP-MP		ICP-MP		CP-MP		AL-MP		s-MCM-41	
	δ_C		δ_C		δ_C		δ_C		δ_C		δ_C		δ_C		δ_C
C1	9.1	C1	8.5	C1	8.7	C1	9.0	C1	8.8	C1	10.5	C1	18.8	C16	22.7
C2	20.6	C2	19.8	C2	19.4	C2	23.1	C2	20.7	C2	18.3	C2	130.8	C15	26.1
C3	42.3	C3	37.2	C3	38.5	C3	42.9	C3	42.2	C3	18.3	C3	114.2	C3−14	29.8
		C5[a]	49.8	C5[b]	49.1	C5	162.2	C5	160.4	C4	118.4			C2	31.8
		C6[a]	45.0	C6[b]	44.5									C1	66.4
				C8[c]	56.1									NCH_3	53.4
				C9[c]	52.2										

[a,b,c] The assignments are somewhat ambiguous for these three pairs of carbons (they may be reversed).

such as postsynthesis grafting[11] and organosiloxane/siloxane co-condensation,[12] need to be improved in order to control the amount and location of the incorporated functional groups. For example, the postsynthesis grafting method typically results in inhomogeneous surface coverage because the introduced organic moieties congregate near the entries to the mesoporous channels and on the exterior surfaces.[13] Although many organically functionalized mesoporous materials were prepared via co-condensation,[13−27] only a few very recent investigations reported that spherical or tubular MCM-41 type silicas could be synthesized via incorporation of mercaptopropyl, allyl, or aminopropyl functional groups.[10,28] Also, the previously reported co-condensation methods usually result in breakup of the structural integrity and long-range periodicity at surface coverages exceeding 25%.

Herein, we report and analyze a new synthetic method that could combine efficient organic functionalization of mesoporous silicas with the control of

(11) Liu, J.; Shin, Y.; Nie, Z.; Chang, J. H.; Wang, L.-Q.; Fryxell, G. E.; Samuels, W. D.; Exarhos, G. J. *J. Phys. Chem. A* **2000**, *104*, 8328−8339.
(12) Stein, A.; Melde, B. J.; Schroden, R. C. *Adv. Mater. (Weinheim, Ger.)* **2000**, *12*, 1403−1419.
(13) Lim, M. H.; Stein, A. *Chem. Mater.* **1999**, *11*, 3285−3295.
(14) Fowler, C. E.; Khushalani, D.; Lebeau, B.; Mann, S. *Adv. Mater. (Weinheim, Ger.)* **2001**, *13*, 649−652.
(15) MacLachlan, M. J.; Asefa, T.; Ozin, G. A. *Chem.-Eur. J.* **2000**, *6*, 2507−2511.
(16) Fowler, C. E.; Burkett, S. L.; Mann, S. *Chem. Commun.* **1997**, 1769−1770.
(17) Fowler, C. E.; Mann, S.; Lebeau, B. *Chem. Commun.* **1998**, 1825−1826.
(18) Hall, S. R.; Fowler, C. E.; Mann, S.; Lebeau, B. *Chem. Commun.* **1999**, 201−202.
(19) Zub, Y. L.; Seredyuk, I. V.; Chuiko, A. A.; Jaroniec, M.; Jones, M. O.; Parish, R. V.; Mann, S. *Mendeleev Commun.* **2001**, 208−210.
(20) Lim, M. H.; Blanford, C. F.; Stein, A. *Chem. Mater.* **1998**, *10*, 467−470.
(21) Lim, M. H.; Blanford, C. F.; Stein, A. *J. Am. Chem. Soc.* **1997**, *119*, 4090−4091.
(22) Babonneau, F.; Leite, L.; Fontlupt, S. *J. Mater. Chem.* **1999**, *9*, 175−178.
(23) Moller, K.; Bein, T.; Fischer, R. X. *Chem. Mater.* **1999**, *11*, 665−673.
(24) Sayari, A.; Hamoudi, S. *Chem. Mater.* **2001**, *13*, 3151−3168.
(25) Inagaki, S.; Guan, S.; Ohsuna, T.; Terasaki, O. *Nature (London)* **2002**, *416*, 304−307.
(26) Burleigh, M. C.; Markowitz, M. A.; Spector, M. S.; Gaber, B. P. *J. Phys. Chem. B* **2001**, *105*, 9935−9942.
(27) Burleigh, M. C.; Markowitz, M. A.; Spector, M. S.; Gaber, B. P. *Chem. Mater.* **2001**, *13*, 4760−4766.

Table 2. ^{29}Si Chemical Shifts (δ_{Si}, in ppm from TMS) and Relative Concentrations of T^n and Q^n Groups Obtained from ^{29}Si DPMAS Spectra

	AP-MP		AAP-MP		AEP-MP		UDP-MP		ICP-MP		CP-MP		AL-MP		s-MCM-41		MCM-41	
	δ_{Si}	%	δ_{Si}	%	δ_{Si}	%	δ_{Si}	%	δ_{Si}	%	δ_{Si}	%	δ_{Si}	%	δ_{Si}	%	δ_{Si}	%
T^2	−59	4	−65	4	−56	1	−62	2	−57	1	−58	2	−64	3				
T^3	−68	8	−69	1	−67	6	−66	4	−66	13	−67	8	−71	8				
Q^2	−93	3	−94	3	−91	3	−91	4	−92	3	−92	2	−97	1	−93	2	−92	3
Q^3	−102	26	−101	28	−101	35	−101	38	−102	29	−101	29	−101	24	−99	34	−101	37
Q^4	−111	59	−111	64	−110	55	−110	52	−111	54	−111	59	−111	64	−110	64	−110	60
SC[a]		29		14		16		13		30		24		33				

[a] SC represents the surface coverage; see text for explanation.

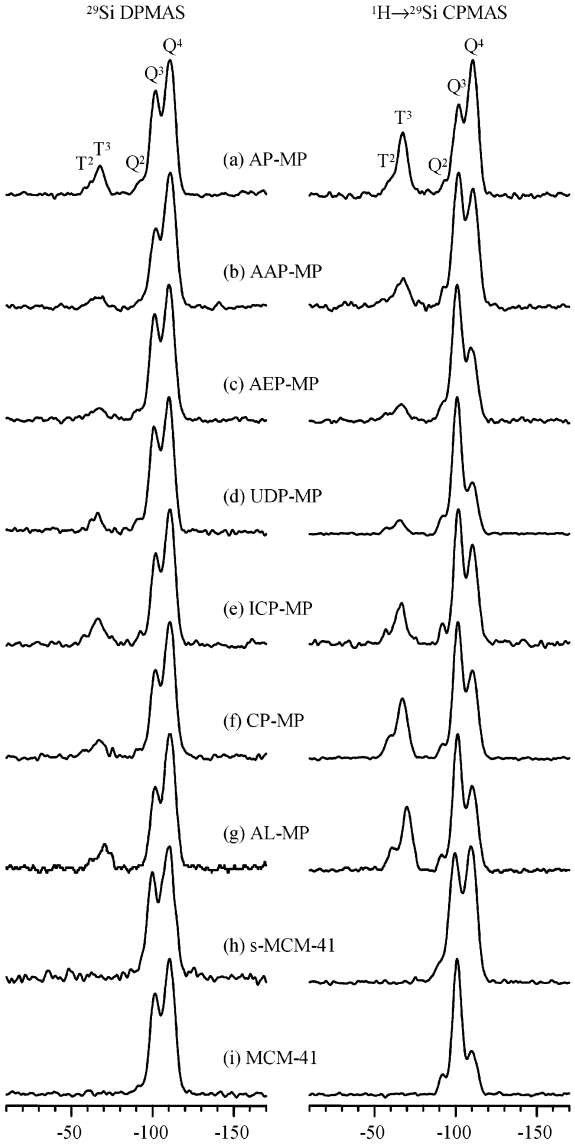

Figure 2. ^{29}Si DPMAS (left) and ^{1}H→^{29}Si CPMAS (right) spectra of AP-MP (a), AAP-MP (b), AEP-MP (c), UDP-MP (d), ICP-MP (e), CP-MP (f), AL-MP (g), s-MCM-41 (h), and MCM-41 after the extraction of surfactant (i).

particle morphology. The degree of functionalization and particle morphology were dictated by the concentration, molecular size, and hydrophilicity/hydrophobicity of the organoalkoxysilane precursors. Our strategy involved a co-condensation method based on sodium hydroxide-catalyzed reactions of tetraethoxysilane (TEOS) with various organoalkoxysilanes in the presence of a low concentration of cetyltrimethylammonium bromide (CTAB) surfactant. The organoalkoxysilanes included 3-aminopropyltrimethoxysilane (APTMS), *N*-(2-aminoethyl)-3-aminopropyltrimethoxysilane (AAPTMS), 3-[2-(2-aminoethylamino)ethylamino]propyltrimethoxysilane (AEPTMS), ureidopropyltrimethoxysilane (UDPTMS), 3-isocyanatopropyltriethoxysilane (ICPTES), 3-cyanopropyltriethoxysilane (CPTES), and allyltrimethoxysilane (ALTMS). In contrast to the Stöber process[29] or the recently reported controlled quenching method,[28] our approach did not involve any organic cosolvents or instantaneous neutralization of alkaline solutions during the co-condensation reaction, respectively. By systematically varying the type and the amount of organoalkoxysilanes, we obtained a series of nanoparticles in the form of spheres, rods, and hexagonal tubes. Throughout this paper, we will refer to these materials as X-MP, where X describes the organoalkoxysilane precursor and MP stands for mesoporous particle. To examine the different mechanistic effects of the organoalkoxysilane-induced shape transformation, we analyzed the structures of these mesoporous organic/inorganic hybrid materials by powder X-ray diffraction (XRD) spectroscopy, field-emission scanning electron microscopy (FE-SEM), nitrogen adsorption−desorption surface analysis (BET isotherms and BJH pore size distributions), and thermogravimetric analysis (TGA). The incorporation of the organic functional groups was quantitatively studied by solid-state NMR spectroscopy of ^{13}C and ^{29}Si. On the basis of the observations of the

Table 3. Structural Properties of the Organically Functionalized Mesoporous Silica Materials

sample	d_{100} (Å)[a]	a_0 (Å)[a]	S_{BET} (m^2/g)[a]	V_p (cm^3/g)[a]	W_{BJH} (Å)[a]	$d_{pore\ wall}$ (Å)[a]	amount of organic groups (mmol/g)[b]
AP-MP	39.8	46.0	721.7	0.45	23.7	22.3	1.7
AAP-MP	41.3	47.7	664.6	0.48	25.9	21.8	0.7
AEP-MP	38.4	44.4	805.8	0.57	26.0	18.4	1.0
UDP-MP	43.7	50.5	1022.4	0.78	28.6	21.9	0.9
ICP-MP	39.8	46.0	840.1	0.66	25.8	20.2	1.5
CP-MP	39.4	45.5	1012.5	0.68	23.5	22.0	1.4
AL-MP	33.7	38.9	1080.5	0.65	19.7	19.2	1.7
MCM-41	38.1	44.0	767.1	0.55	25.5	18.5	

[a] The BET surface area (S_{BET}), the mesopore volume (V_p), and the mean mesopore width (W_{BJH}) were obtained from the nitrogen adsorption/desorption data. The d_{100} numbers represent the *d*-spacing corresponding to the main (100) XRD peak. The unit cell size (a_0) is calculated from the d_{100} data using the formula $a_0 = 2d_{100}/3^{1/2}$. The pore wall thickness $d_{pore\ wall} = a_0 - W_{BJH}$. [b] The amounts of organic functional groups incorporated to the silica materials were estimated from the ^{29}Si DPMAS.

(28) Sadasivan, S.; Khushalani, D.; Mann, S. *J. Mater. Chem.* **2003**, *13*, 1023−1029.
(29) Stoeber, W.; Fink, A.; Bohn, E. *J. Colloid Interface Sci.* **1968**, *26*, 62−69.

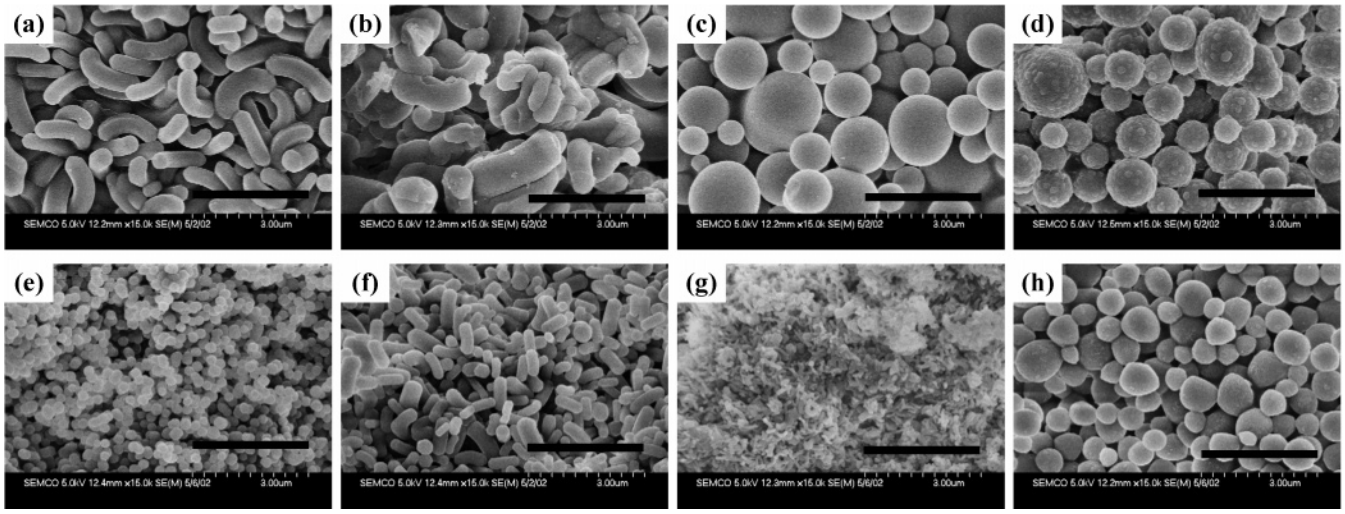

Figure 3. FE-SEM images of AP-MP (a), AAP-MP (b), AEP-MP (c), UDP-MP (d), ICP-MP (e), CP-MP (f), AL-MP (g), and pure MCM-41 silica (h) synthesized via our condensation reaction condition without adding any organic functional group. All images are presented using the same scale, with the scale bar = 3 μm.

morphological structures and the degree of organic functionalization, we proposed a formation mechanism of mesoporous silica nanoparticles with different morphologies that relies on the interaction between organoalkoxysilanes and CTAB micelles.

Experimental Section

The organoalkoxysilane precursors used for our co-condensation reactions contain a common trimethoxysilyl or triethoxysilyl terminal group and different organic functional groups, as depicted in Scheme 1. APTMS, AAPTMS, AEPTMS, UDPTMS, ICPTES, CPTES, ALTMS, TEOS, and CTAB were purchased from Aldrich and used as received. The reaction mixture contained CTAB/TEOS/organotrialkoxysilane of choice (unless specified otherwise)/NaOH/H_2O (1.0:8.16:1.05:2.55:4857) based on the molar ratio. For example, in the case of AP-MP, the mixture of CTAB (2.0 g, 5.49 mmol), 2.0 M of NaOH(aq) (7.0 mL, 14.0 mmol), and H_2O (480 g, 26.67 mol) was heated at 80 °C for 30 min to reach pH 12.3. To this clear solution, TEOS (9.34 g, 44.8 mmol) and APTMS (1.03 g, 5.75 mmol) were added sequentially and rapidly via injection. Following the injection, a white precipitation was observed after 3 min of stirring at ca. 550 rpm. The reaction temperature was maintained at 80 °C for 2 h. The products were isolated by a hot filtration, washed with copious amount of water and methanol, and dried under vacuum. The reaction yields of as-made products varied with respect to the choice of organoalkoxysilane and ranged from 38 to 65% of the starting weight of TEOS. An acid extraction was performed in a methanol (100 mL) mixture of concentrated hydrochloric acid (1.0 mL) and as-made materials (1.0 g) at 60 °C for 6 h. Resulting surfactant-removed solid products were filtered and washed with water and methanol, and then dried under vacuum. Pure MCM-41 samples were prepared as reference using the same experimental conditions. The as-synthesized sample containing the surfactant will be referred to as s-MCM-41, while the sample with CTAB removed will be simply denoted as MCM-41.

Particle morphology of these materials was determined by scanning electron microscopy (SEM) using a Hitachi S4700 FE-SEM system with 10 kV accelerating voltage and 0.005 nA of beam current for imaging. For transmission electron microscopy (TEM) studies, a small aliquot was taken from a suspension of methanol and placed in a lacey carbon-coated TEM grid, which was pulled through the suspension and allowed to dry in air. Thin sections of samples embedded in epoxy resin were obtained with ultramicrotomy (60−80 nm). The resulting sample was examined with a Philips model CM-30 TEM operated at 300 kV. The specimen was given no further treatment, as it appeared stable under beam bombardment.

Powder XRD experiments were performed on a Scintag XDS 2000 diffractometer using a Cu Kα radiation source. Low angle diffraction with a 2θ range of 1 to 10° was used to investigate the long-range order of the materials. The surface area and median pore diameter were measured using N_2 adsorption/desorption measurements in a Micromeritics ASAP 2000 BET surface analyzer system. The data were evaluated using the Brunauer−Emmett−Teller (BET) and Barrett−Joyner−Halenda (BJH) methods to calculate the surface area and pore volumes/pore size distributions, respectively. Samples were prepared by degassing at 90 °C for 1 h and then at 150 °C for 4 h. TGA curves were recorded using a TA Instruments TGA 2950 thermogravimetric analyzer with a temperature ramp of 5 °C/min under continuous flow of nitrogen (100 mL/min).

Solid-state nuclear magnetic resonance (NMR) experiments were performed on a Varian/Chemagnetics Infinity spectrometer at the frequencies of 79.5, 100.6, and 400.0 MHz for ^{29}Si, ^{13}C, and ^{1}H nuclei, respectively. ^{13}C and ^{29}Si nuclei were observed using direct polarization (DP) or by cross polarization[30] (CP) from the neighboring ^{1}H nuclei. The samples were placed in 5-mm zirconia rotors and spun at 10 kHz in a doubly tuned Chemagnetics probe. The saturation recovery experiment, carried out for AL-MP and ICP-MP samples, yielded the ^{29}Si longitudinal relaxation times in the range of 30 to 65 s. Despite slow relaxation, ^{29}Si DPMAS measurements were performed to obtain quantitative spectra for all samples. These experiments used excitation with a single 90° pulse of 2.1 μs followed by data acquisition under continuous wave (CW) ^{1}H decoupling at 65 kHz. Typically 270 scans were completed using a pulse delay of 300 s.

The variable amplitude CPMAS scheme[31] was used to enhance the polarization of observed nuclei and increase the repetition rate of data acquisition. During each cross polarization period, the ^{1}H rf field was ramped between 16 and 40 kHz using 2.4 kHz increments, whereas the ^{29}Si (or ^{13}C) rf field was maintained at a constant level of approximately 36 kHz. The maximum ^{1}H→^{29}Si polarization transfer was achieved using a contact time of approximately 10 ms, which is in agreement with previous studies performed for silicas.[32,33] For

(30) Pines, A.; Gibby, M. G.; Waugh, J. S. *J. Chem. Phys.* **1973**, *59*, 569−590.
(31) Peersen, O. B.; Wu, X.; Kustanovich, I.; Smith, S. O. *J. Magn. Reson. A* **1993**, *104*, 334−339.
(32) Maciel, G. E.; Sindorf, D. W. *J. Am. Chem. Soc.* **1980**, *102*, 7606−7607.
(33) Sindorf, D. W.; Maciel, G. E. *J. Am. Chem. Soc.* **1983**, 105, 3767−3776.

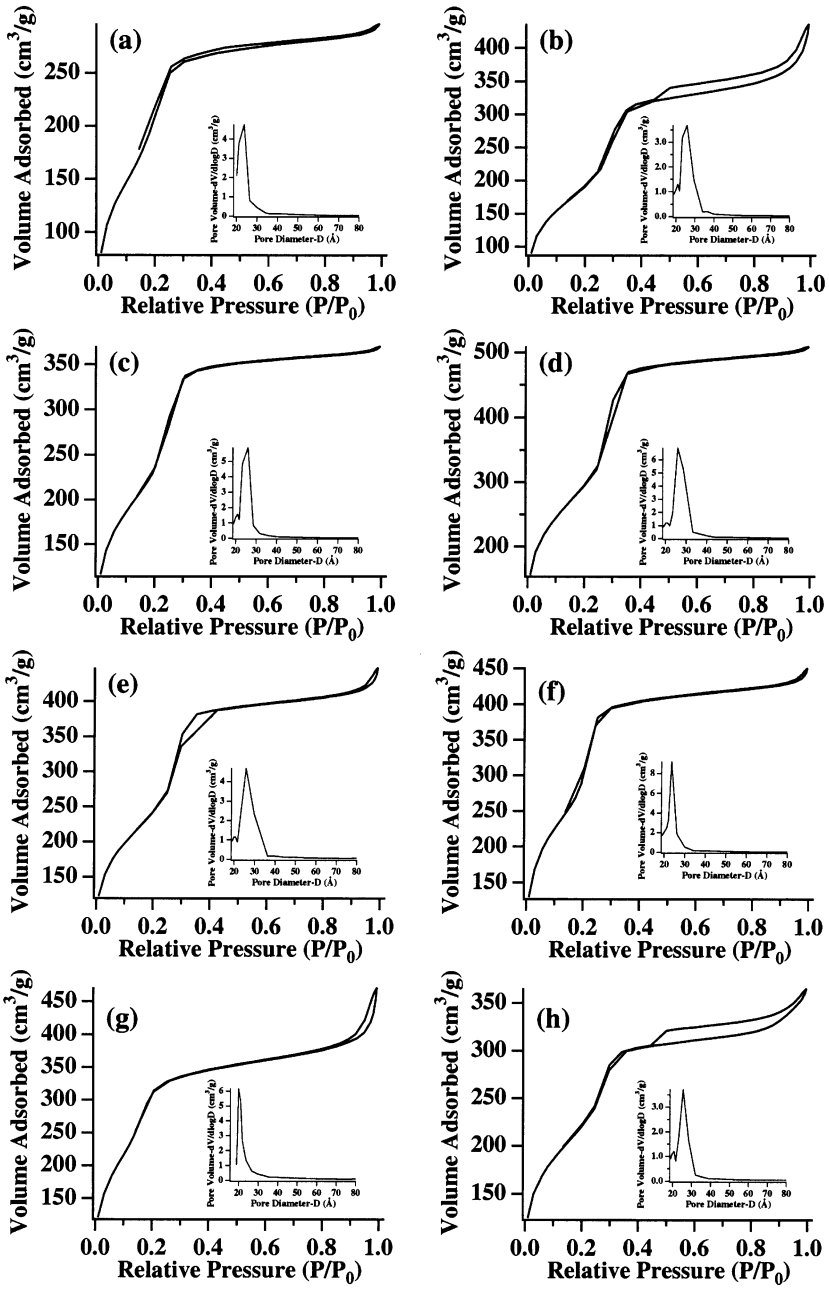

Figure 4. BET isotherms and BJH pore size distributions (insets) of AP-MP (a), AAP-MP (b), AEP-MP (c), UDP-MP (d), ICP-MP (e), CP-MP (f), AL-MP (g), and pure MCM-41 silica (h) materials.

^{13}C nuclei, shorter contact times of 0.4−1.5 ms were used. The ^{1}H rf magnetic fields of 90 kHz and 65 kHz were used for initial excitation and decoupling, respectively. The values of ^{1}H longitudinal relaxation time encountered in all mesoporous samples examined in this study did not exceed 1 s, which allowed for repetition time of 1.2 s to be used in the CPMAS experiments. Typically, 4K scans were accumulated for $^{1}H \rightarrow ^{29}Si$ CPMAS, whereas $^{1}H \rightarrow ^{13}C$ experiments required between 1K and 10K scans per spectrum. All chemical shifts were referenced to $SiMe_4$.

Results and Discussion

Organic Functionalization. To simplify the analysis, we initially prepared a series of samples in which the amount of organoalkoxysilane used for the preparation was fixed at 12.8 mol % of the amount of TEOS. The $^{1}H \rightarrow ^{13}C$ CPMAS spectra of these samples, shown in Figure 1, provide clear evidence that they were indeed functionalized as intended. The observed chemical shifts, listed in Table 1, agreed well with those observed in homogeneous solutions of the corresponding precursors and were easily assigned. For example, the resonances at 6.5 and 45.3 ppm in the spectrum of APTMS dissolved in $CDCl_3$ (not shown) corresponded to those at 9.1 ppm (C1) and 42.3 ppm (C3) observed in AP-MP. The resonance at 28 ppm representing C2 exhibited a larger shift change toward higher field relative to the liquid state (20.6 ppm). The CPMAS spectrum of s-MCM-41 sample (Figure 1h) consisted of several resonances due to CTAB, among which the peak at around 30 ppm, corresponding to carbons C3 through C14, was most intense. Two samples, CP-MP and AL-MP, contained detectable resonances from CTAB (marked with

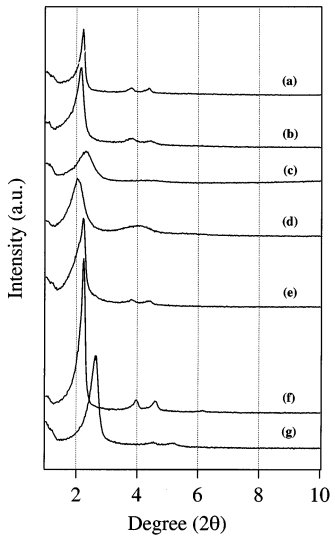

Figure 5. XRD spectra of the surfactant-removed AP-MP (a), AAP-MP (b), AEP-MP (c), UDP-MP (d), AL-MP (e), CP-MP (f), and ICP-MP (g).

asterisks in spectra f and g), which comprised just a few % of the total ^{13}C intensity.

The functionalization of silicas was further studied by TGA and solid-state NMR of ^{29}Si (Figure 2 and Table 2). In general, three or four distinct weight loss TGA profiles were found, including methanol, organic functional groups, and a small weight loss due to the dehydration of the surface hydroxyl groups. Although the TGA data provided evidence of the existence of organic functional groups inside the pores, a direct, quantitative measure of the organic functionalization was provided by ^{29}Si DPMAS spectra shown in the left column of Figure 2. The resonances at around −59 and −68 ppm represented silicon atoms in positions $(\equiv SiO)_2\mathbf{Si}(OH)R$ and $(\equiv SiO)_3\mathbf{Si}R$, which are denoted T^2 and T^3, respectively.[33−36] These silicon species were better observed using the ^{29}Si CP-MAS NMR method (Figure 2, right column), which detected only the nuclei located within 2−3 bond lengths from the nearest hydrogen atoms. Note that the presence of T^3 and T^2 functionalities confirmed the existence of the covalent linkage between the organic groups and the silica surface. The resonance lines representing Q^4 (siloxane, $(\equiv SiO)_4\mathbf{Si}$)), Q^3 (single silanol, $(\equiv SiO)_3\mathbf{Si}OH$), and Q^2 (geminal silanol, $(\equiv SiO)_2\mathbf{Si}(OH)_2$) silicons were also

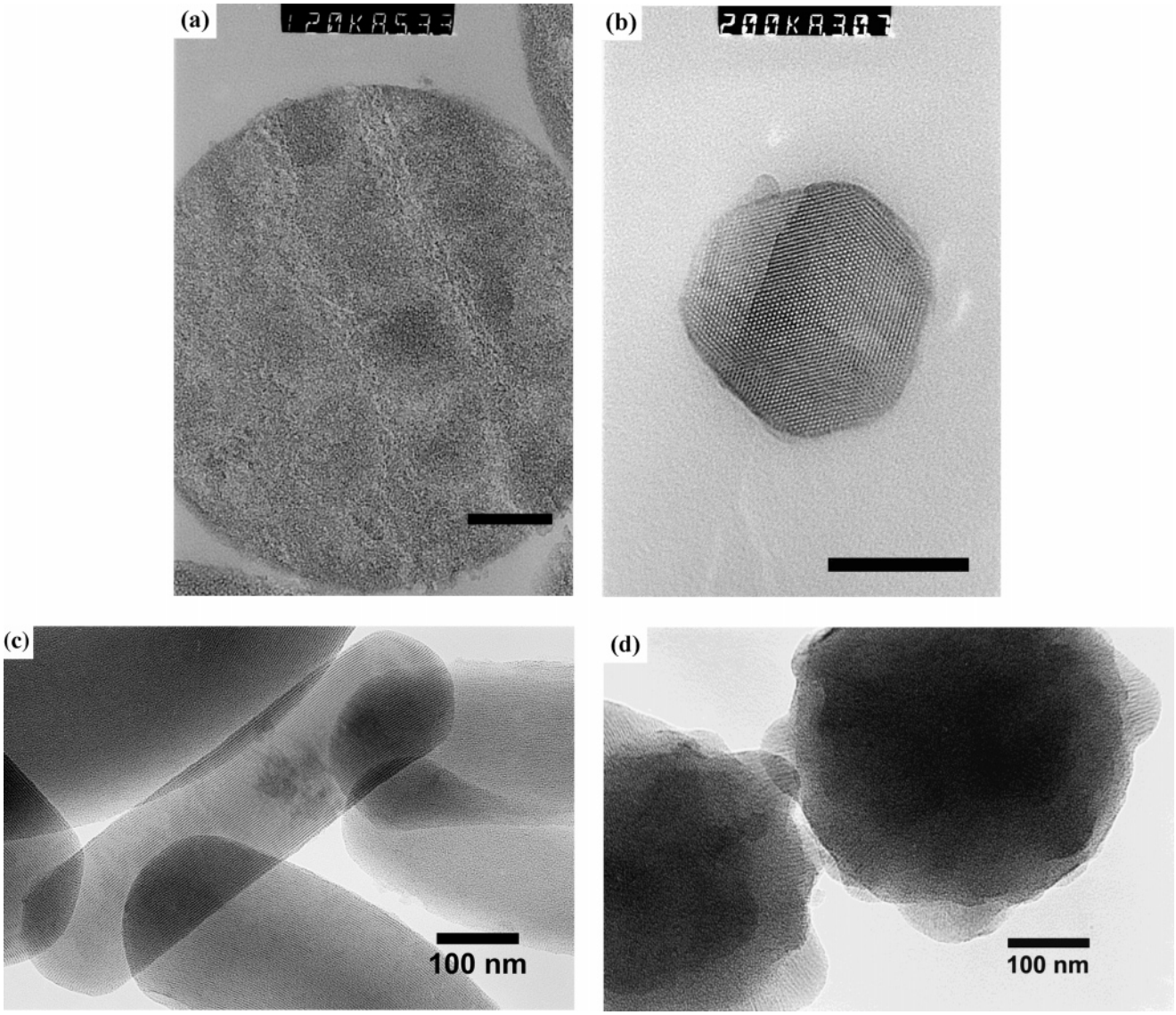

Figure 6. TEM micrographs of AEP-MP (a), CP-MP (b, c), and UDP-MP (d) materials. Images (a) and (b) represent ultramicrotomed samples (all scale bars = 100 nm).

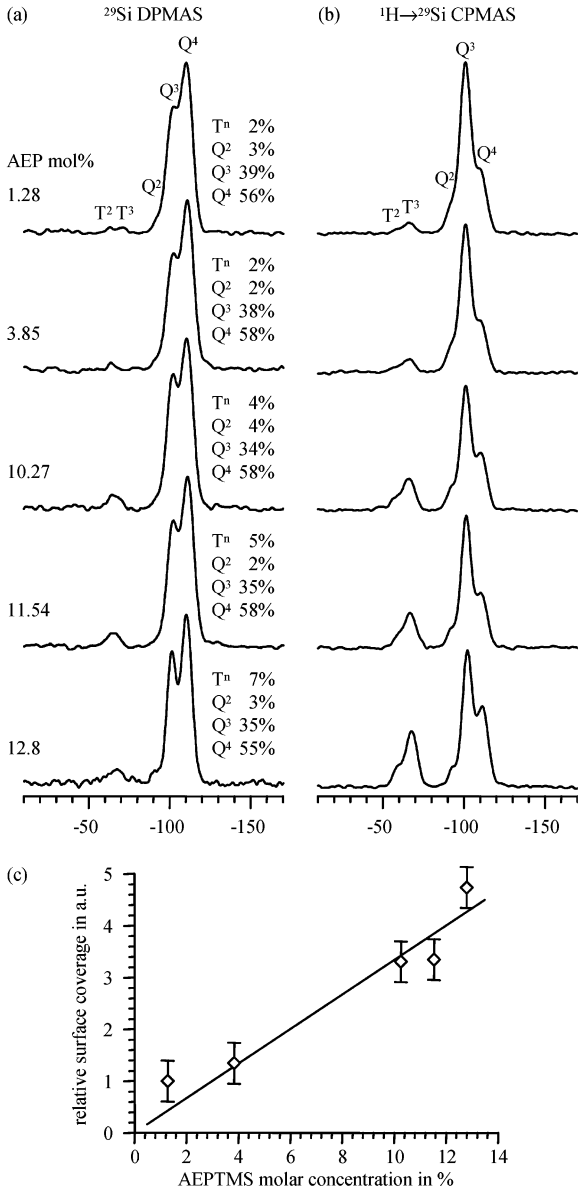

Figure 7. ^{29}Si DPMAS (a) and ^{1}H→^{29}Si CPMAS (b) spectra of functionalized mesoporous materials with various amounts of AEPTMS. A contact time of 1 ms was used during cross polarization period. (c) The relative increase of functionalization versus the concentration of AEPTMS estimated from CPMAS.

observed in their usual spectral positions.[32−36] The relative concentrations of all silicon sites were obtained by deconvolution of DPMAS spectra (see Table 2). Assuming that all Q^3 and Q^2 sites decorated the interior walls of mesoporous silicas, the surface coverage (SC) of the mesopores with organic moieties could be estimated as $SC = (T^2 + T^3)/(Q^2 + Q^3 + T^2 + T^3)$. As shown in Table 2, the SC values varied between 13% for UDP-MP and 33% for AL-MP. The measured loading efficiencies of the MPs synthesized with the organoalkoxysilanes containing hydrophobic functional groups, such as CPTES and ALTMS, were higher than those that contained the hydrophilic precursors, such as AAPTMS and AEPTMS. These results suggested that the organoalkoxysilanes with hydrophobic functional groups could better orient themselves around the water/micelle interface and intercalate these groups to the hydrophobic regions of the CTAB micelles during the co-condensation reactions.

Morphology Control. The morphology and mesoporous structure of the organically functionalized MP materials were studied using FE-SEM and powder X-ray diffraction. The FE-SEM micrographs demonstrated a variety of particle shapes and sizes. For example, the AP-MP material showed a curved hexagonal shaped tubular morphology, as depicted in Figure 3a. Interestingly, upon replacing the APTMS with other structurally similar organoalkoxysilanes, such as AAPTMS and AEPTMS (Figure 3b and c), the shapes transformed into twisted columns and micrometer-sized spheres, respectively. In contrast to the smooth particle surface of AEP-MP, UDP-MP (Figure 3d) exhibited micron-sized spherical particles with raspberry-like bumpy rough surfaces. The ICP-MP material (Figure 3e) consisted of the smallest spherical particles with diameters ranging from 100 to 500 nm. In the synthesis of CP-MP (Figure 3f) and AL-MP materials (Figure 3g), hexagonal rod-shaped particles of different lengths and diameters were observed. The average particle size of CP-MP (1 μm long and 500 nm diameter) is larger than that of AL-MP (500 and 50 nm, respectively). As a rule, the particle sizes of materials prepared with the hydrophobic organoalkoxysilane precursors, such as ICPTES, CPTES, and ALTMS, appear significantly smaller than pure MCM-41 (Figure 3h), whereas the materials synthesized with more hydrophilic organoalkoxysilanes, such as AAPTMS, AEPTMS, and UDPTMS, yielded larger particles. Note that the co-condensation reactions took place in a basic aqueous solution (pH = 12.3), therefore the trialkoxysilyl groups of these organoalkoxysilanes were hydrolyzed and converted to the trihydroxysilyl group, which is always hydrophilic. The other end of the molecule can be either hydrophilic or hydrophobic depending on the water solubility of the organic functional group involved.

The surface areas, pore volumes, and pore size distributions of the MP materials were analyzed by nitrogen adsorption−desorption techniques. As shown in Figure 4, all silicas exhibited characteristic Type IV BET isotherms consistent with the presence of cylindrical *meso*-scale pores. However, as outlined in Table 3, the BJH average pore diameters were different depending on the types of the incorporated organic functional groups. Again, utilization of the hydrophobic precursors yielded smaller pores. The powder XRD spectra of these materials (Figure 5) featured an intense (100) reflection peak corresponding to lattice spacings in the range of 33.7 to 43.7 Å. Even though (210) peaks were not observed, the well-resolved diffraction patterns characteristic of hexagonal MCM-41 silicas,[37] including (100), (110), and (200) peaks with the spacing ratio of $1:\sqrt{3}:\sqrt{4}$, were observed in AP-MP, AAP-MP, CP-MP, ICP-MP, and AL-MP. On the other hand, AEP-MP and

(34) Maciel, G. E. In *Encyclopedia of Nuclear Magnetic Resonance*; Grant, D. M., Harris, R. K., Eds.; John Wiley & Sons Ltd: Chichester, 1996; Vol. 7, pp 4370−4386.
(35) Engelhardt, G.; Michel, D. *High-Resolution Solid-State NMR of Silicates and Zeolites*; John Wiley & Sons: Chichester, 1987.
(36) Lindner, E.; Schneller, T.; Auer, F.; Mayer, H. A. *Angew. Chem., Int. Ed.* **1999**, *38*, 2155−2174.
(37) Gulik, A.; Delacroix, H.; Krischner, G.; Luzzati, V. *J. Physique II* **1995**, *5*, 445−464.

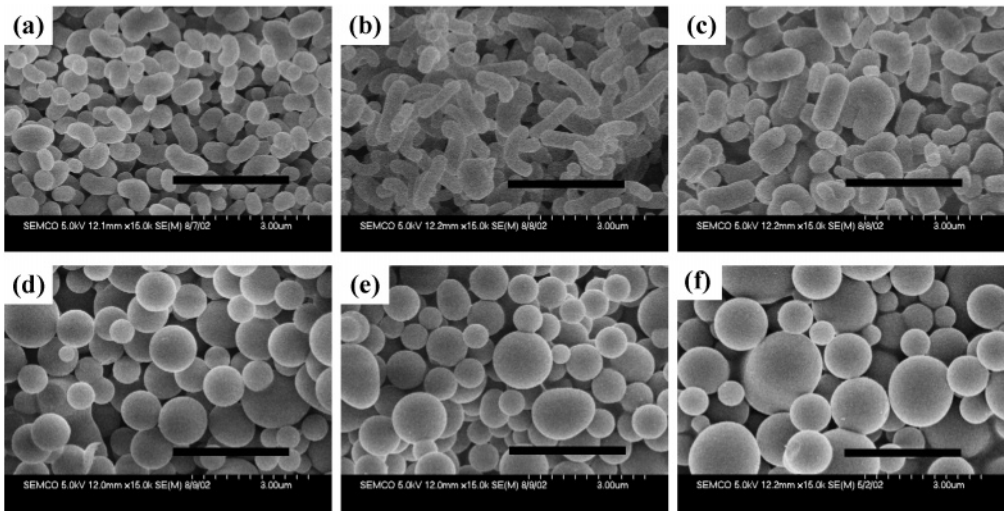

Figure 8. FE-SEM images of AEP-MPs with different initial loadings of AEPTMS: 1.28 (a), 3.85 (b), 6.43 (c), 10.27 (d), 11.54 (e), and 12.80 mol % (f). All images are presented using the same scale, with the scale bar = 3 μm.

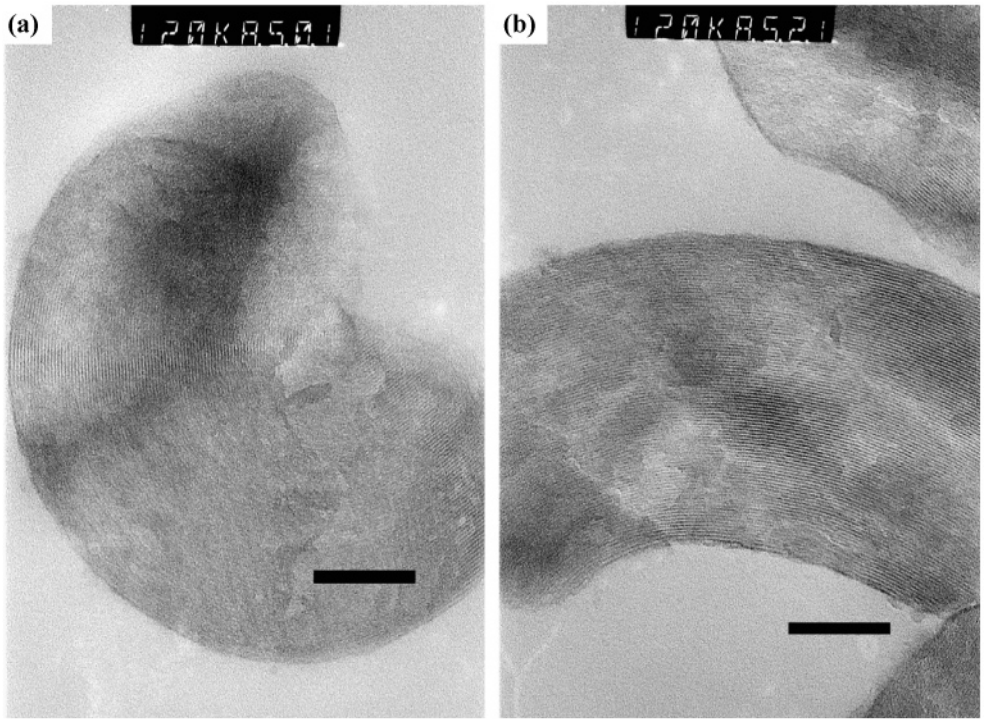

Figure 9. TEM images of ultramicrotomed AEP-MPs with 1.28 mol % (a) and 6.43 mol % (b) AEPTMS (scale bar = 100 nm).

UDP-MP (Figure 5c and d) appeared to be disordered as evidenced by broad peaks at 4.52° and 4.10°, respectively, representing superimposed (110) and (200) patterns. The TEM micrographs of these samples shown in Figure 6a and d are consistent with this observation. In contrast, the TEM micrographs of materials prepared with hydrophobic organoalkoxysilanes, such as CPTES, showed well-organized mesopores packed in hexagonal symmetry as evidenced in Figure 6b and c.

Mechanism Responsible for the Shape Formation. As discussed earlier, similar organic precursors can yield very different particle morphologies, e.g., AAP-MP showed tubular-shaped particles (Figure 3b) whereas the AEP-MP exhibited exclusively spherical particles (Figure 3c). Clearly, several different interactions, such as electrostatic attraction/repulsion, hydrogen bonding, and hydrophobic interaction, between the organoalkoxysilanes and surfactant molecules at the micelle/water interface could contribute cooperatively to the observed drastic changes in particle morphology. We undertook an approach of deconvoluting some of these factors by investigating how the concentration of a selected organoalkoxysilane (AEPTMS) could influence the resulting particle shape and size. The molar ratio of AEPTMS/TEOS was systematically varied from 1.28 to 12.8 mol %, while the concentrations of all the other chemicals introduced to the co-condensation reaction were fixed at the previously described levels. The incorporation of AEP was quantitatively determined by DPMAS and CPMAS ^{29}Si NMR (Figure 7a and b). As discussed earlier, the DPMAS spectra provided quantitative measure of the relative concentrations of Q^n and T^n functionalities. However, due to a low concentration of T^n species, the SC values were not directly measured in this series of samples. Instead, we used the CPMAS spectra to evaluate the relative change of T^n intensities

Scheme 2

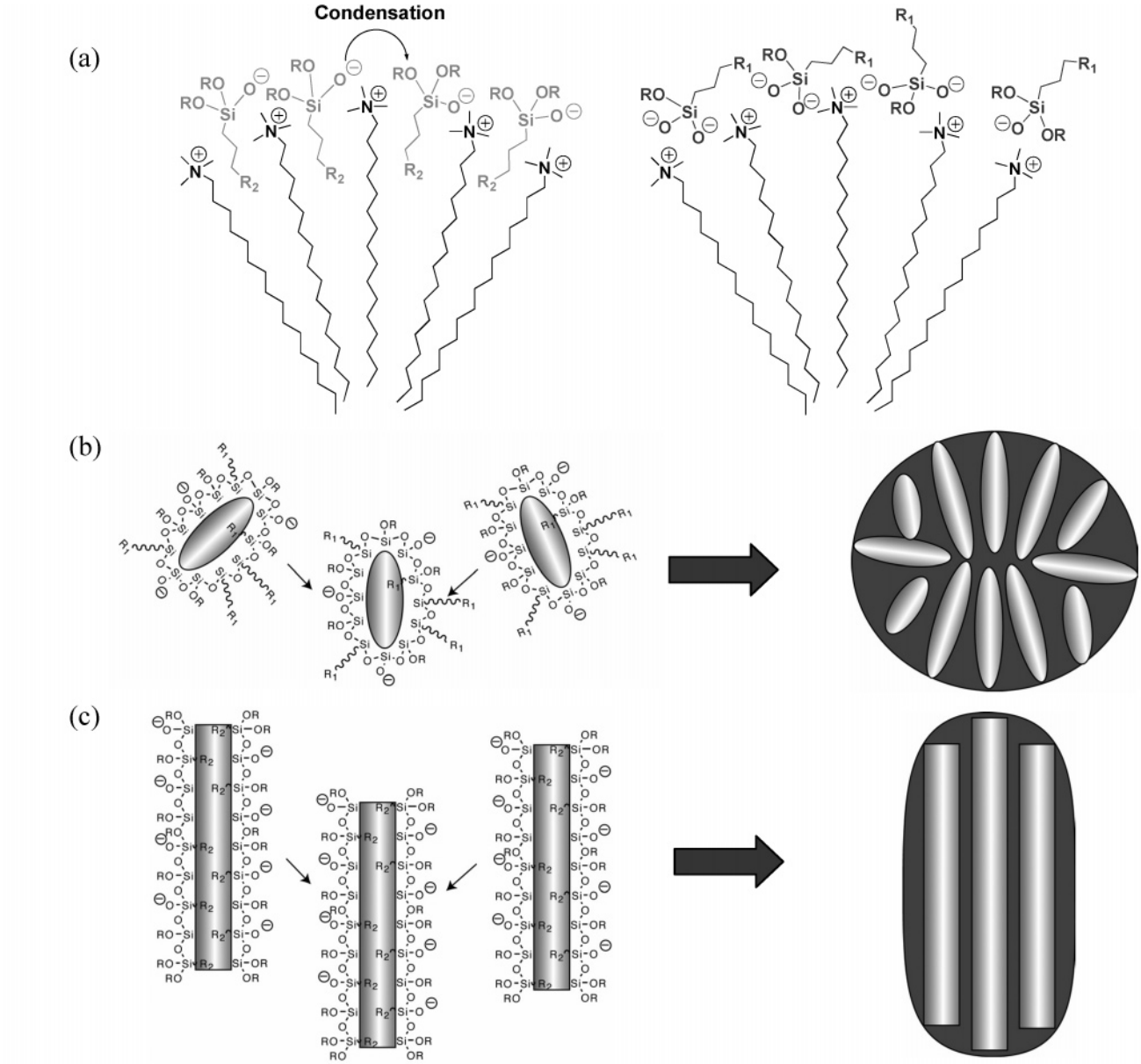

R = Methyl or Ethyl groups; R_1 = Hydrophilic functional groups; R_2 = Hydrophobic functional groups

versus the concentration of AEPTMS. The results, plotted in Figure 7c in reference to the sample with 1.28 mol % of AEPTMS, showed that the concentration of AEP increased almost linearly as the initial AEPTMS/TEOS molar ratio changed from 1.28 to 12.8 mol %. The particle morphology and mesoporous structures of the resulting materials were analyzed by FE-SEM and TEM. The FE-SEM micrographs of Figure 8 show a concurrent transformation of the particle morphology from small kidney-bean-shaped rods to spheres, with elongated rods and ellipsoidal particles being observed at intermediate concentrations of AEPTMS. Furthermore, a noticeable increase of the average particle sizes of these materials could be observed at higher concentrations of AEPTMS. The TEM micrographs (Figure 9a and b) of the AEP-MP materials with low degrees of functionalization (1.28 and 6.43 mol %, respectively) revealed that the mesopores are uniformly aligned along the long axes of MP's despite their different particle sizes. This is in contrast to the randomly oriented mesopores observed in the spherical AEP-MP's with the higher degree of functionalization (Figure 6a).

On the basis of these results, the following mechanism is proposed to account for the formation of different particle shapes and sizes. To facilitate the ensuing discussion, we present Scheme 2 where R_1 and R_2 represent the hydrophilic and hydrophobic functional groups, respectively. In the case of the more hydrophobic organoalkoxysilane precursors, such as CPTES and ALTMS, the aforementioned strong interaction between their nonpolar groups (R_2) and the hydrophobic hydrocarbon tails of the CTAB molecules could likely stabilize the formation of long individual cylindrical micelles by intercalating their hydrophobic groups to the micelles, as shown in Scheme 2b. The uniform organization of the trialkoxysilyl group at the Gouy−Chapman region of the surface of micelles and their increased length would assist in the rapid cross-linking/condensation between the "micelle-oriented" trialkoxysilyl groups in the basic NaOH aqueous solution, as depicted in Scheme

2c. The resulting "side-on" packing of the silicate-coated cylindrical micelles would give rise to small rodlike nanoparticles. Similar phenomenon has been observed by Cai et al.[38] while utilizing NaOH and NH_4OH as catalysts to manipulate the particle morphology of the MCM-41 silicas without organic functional groups. The above mechanism would not be operable for more hydrophilic organoalkoxysilane precursors, such as AAPTMS, AEPTMS, and UDPTMS, because their R_1 functional groups are not favored by the interaction with the surfactant molecules (Scheme 2a). This would inhibit the formation of long micelles and reduce their tendency toward side-on condensation. The difference in rate of condensation between silicate-coated micelles versus that of the free silicate (TEOS) molecules would be small. Because of the lack of thermodynamic incentives for the silicate-coated micelles to pack in an ordered fashion, such co-condensation reactions should yield particles with randomly oriented pore structures. This hypothesis was supported by our study of synthesizing AEP-MPs with different concentrations of AEPTMS. The fact that the spherical-shaped AEP-MP obtained with 12.8 mol % AEPTMS showed disordered mesoporous structure indicated that the amount of hydrophilic precursors introduced was perhaps high enough to disturb the side-on growth mechanism. A similar phenomenon was recently reported by Mann and co-workers,[28] who observed the growth of the mesoporous silica particle in the direction that is perpendicular to the pore-alignment upon the introduction of amine-containing organoalkoxysilanes. At lower concentrations of AEPTMS, rod-shaped materials were generated with small average particle sizes, which indicated that the disruption of the packing mechanism was indeed minimized.

(38) Cai, Q.; Luo, Z.-S.; Pang, W.-Q.; Fan, Y.-W.; Chen, X.-H.; Cui, F.-Z. *Chem. Mater.* **2001**, *13*, 258−263.

Conclusions

In this study, we have demonstrated that a series of organically functionalized MCM-41 type mesoporous silicas with various particle morphologies could be synthesized by a co-condensation method. The co-condensation reactions used various amounts of organoalkoxysilanes with different functional groups as structure-directing reactants. The mechanism responsible for the observed changes in particle morphology and pore alignment has been proposed. Further studies of this mechanism, which will also include the size effect of the organoalkoxysilane precursors, will be performed. Better understanding of such synthetic strategies and the underlying mechanisms of functionalization and morphology control will lead to construction of various sophisticated organic/inorganic hybrid nanomaterials for heterogeneous sensors and catalysts with high selectivity and efficiency.

Acknowledgment. V. S.-Y. Lin thanks the NSF (Career Award CHE-0239570) and the Green Chemistry Catalysis Laboratory (GCCL) of the U.S. DOE Ames Laboratory for financial support of this work. This research was also supported at Ames Laboratory by the U.S. Department of Energy, Office of Basic Energy Sciences, Division of Chemical Sciences, under Contract W-7405-Eng-82.

CM0210041